Contents lists available at ScienceDirect

International Journal of Heat and Mass Transfer

Numerical modelling of hyperbolic phase change problems: Application to continuous casting

Youssef Belhamadia [a,*], Guilherme Ozorio Cassol [b], Stevan Dubljevic [b]

[a] *American University of Sharjah, Department of Mathematics and Statistics, Sharjah, United Arab Emirates*
[b] *University of Alberta, Chemicals and Materials Engineering Department, Alberta, Canada*

ARTICLE INFO

ABSTRACT

Heat diffusion processes are generally modeled based on Fourier's law to estimate how the temperature propagates inside a body. This type of modeling leads to a parabolic partial differential equation, which predicts an infinite thermal wave speed of propagation. However, experimental evidence shows that diffusive processes occur with a finite velocity of thermal propagation in many applications. In this paper, we develop a mathematical formulation to predict the finite speed of heat propagation in multidimensional phase change problems. The model generalizes the enthalpy formulation by adding a hyperbolic term. The governing equations are simulated by the finite element method. The proposed model is first verified by comparing numerical and experimental results illustrating the difference between the infinite and finite propagation velocity for heat inside biological tissues. Then, the results of the two and three-dimensional numerical solution of the continuous steel casting process are presented. We will illustrate that the effects of the initial conditions vanish faster when using the parabolic equation, while they persist in the hyperbolic modeling approach. The results demonstrate significant differences in the initial thermal dynamics and at the solid-liquid interface position when adding the hyperbolic term. The changes are more noticeable in the regions of the steel beam where rapid heat loss and, consequently, faster phase change occur.

1. Introduction

Heat transfer is one of the most fundamental problems studied when considering energy transport. Given a temperature difference in a body, heat flows until thermal equilibrium is reached. The flow, in this case, is called heat conduction, a phenomenon related to the direct microscopic exchange of kinetic energy between the particles in the body. Regarding heat transfer modeling, the conductive heat transport across the macroscopic scale is generally described by a parabolic partial differential equation (PDE) obtained by defining the heat flux given by Fourier's law. In Fourier's law, an initial temperature gradient in a conductive medium causes an immediate heat flux and instantly propagates throughout the body but still decays exponentially [1]. However, this issue cannot be ignored in some applications, and using a parabolic equation may be inaccurate enough for practical purposes. Experimental evidence shows that diffusive processes occur with a finite velocity

of thermal propagation inside matter, such as materials with non-homogeneous structures [2], nano-wires or nano-structure materials [3], and materials subjected to extremely fast thermal disturbances [4,5].

Several contributions have addressed the paradox of infinite propagation speed over the years. Most of these consider either a hyperbolic or a nonlinear parabolic equation as the system model. Based on the kinetic theory, Cattaneo proposed, in Cattaneo [6], a modified flux that took into account thermal inertia, resulting in a hyperbolic equation when applied to the energy balance. This type of model was later on also derived based on Boltzmann's equation [7] or using the correlated random walk [8]. In King et al. [9] and Novikov et al. [10], the numerical and analytical solutions of the hyperbolic heat equation in an infinite space were shown.

Although the hyperbolic equation can be seen as an extension of the parabolic model, there have been several contributions deriving other models from it or criticizing its use, showing the limitations and restrictions of different lagged heat flux models. In [11], the relaxed flux was considered for heat conductor models with fading memory by different approximations of dual-phase-lag

theory. While assuming an approximate constitutive equation for the heat flux, the parametric limitations on the equations obtained were analyzed. In [12], it was shown that using a telegrapher's equation is not a fitting solution for transport problems in more than one dimension. Similarly, Rukolaine [13] showed in their simulations that a type of lagged heat flux model might present a nonphysical solution for different values of the parameters. The contributions from Bright and Zhang [14], Maillet [15] criticize models using Cattaneo and Vernotte hyperbolic heat equation or derived from it, stating assumptions as to why some previous published experimental results might have been biased and not accurate. Finally, in Both et al. [16], a heat pulse experiment at room temperature was conducted, showing that the results could not be modeled properly either by the Fourier or non-Fourier approaches.

Nonetheless, there are several recent contributions that still use the hyperbolic approach and show that a Fourier heat flux is not able to describe some systems properly. In [17–20], the hyperbolic type model was used to model the propagation on a heterogeneous mixture to predict the effect of extremely fast thermal disturbances in microscopic sliding contact, to estimate the heat propagation in biological tissues, and to model the finite speed of propagation seen in cardiac electrophysiology, respectively. More recently, the thermal behavior of hyperbolic conduction semi-spaces in perfect thermal contact was investigated in Nosko [21]. In [22], the analytical solution of a non-Fourier model was used to describe the temperature behavior obtained when using a heat pulse method on different rock samples, a continuation of the work previously shown in Both et al. [16]. Thus, even though the hyperbolic equation might have fundamental limitations, its utility as an empirical model is evident.

One type of heat transfer problem is related to the phase change phenomenon, where the material state is transformed from solid, liquid, or gas to another state without a change in chemical composition. Phase change problems have been the subject of many experimental and theoretical studies. The classical two-phase Stefan formulation is considered for the mathematical equation representing these problems. In this formulation, the heat is modeled on each phase separately while the interface, the boundary between different phases, is considered without any a priori knowledge of its dynamics [23].

For phase change problems, the hyperbolic Stefan problem has been considered in some contributions in the literature. In Socio et al. [24], the difference between the Fourier and non-Fourier models of heat conduction associated with a change of phase in a solid material has been investigated. In Showalter et al. [25], the enthalpy formulation corresponding to the hyperbolic Stefan problem has been discussed. In Glass et al. [26], the enthalpy formulation of the hyperbolic Stefan problem has been used to analyze the effects of the Stefan number and thermal conductivity on the propagation of the phase change interface. Recently, in Jitendra et al. [27], a numerical solution of a non-Fourier heat conduction model has been applied to the phase change problem in the presence of variable internal heat generation.

Most of the aforementioned references considered only one-dimensional cases of the phase change problem. For multi-dimensional cases, numerical simulation of the Stefan problem is challenging due to the explicit imposition of the Stefan condition on the interface. To our knowledge, only Kumar et al. [28] where a two-dimensional hyperbolic phase change heat transfer process in cryosurgery of the lung has been presented, where the enthalpy formulation was used, and the governing equations were solved by a finite difference method.

The main goal of this paper is to present a multi-dimensional formulation and numerical technique for solving the hyperbolic phase change problem. Specifically, the model and numerical method are used to simulate the continuous casting process, an eco-friendly method that enhances the production of metals and is the most important production process in the steel industry. Thus, first, a novel formulation based on the enthalpy technique is developed to solve the hyperbolic classical Stefan problem. The main advantage of this approach is that both solid and liquid temperatures are solved in the entire domain, and the Stefan condition is automatically satisfied at the interface. For the numerical solution of the proposed formulation, a finite element method is considered. A comparison between numerical and experimental results illustrating the difference between the infinite and finite propagation velocity for heat inside biological tissues is first presented. Then, two and three-dimensional simulations are presented, showing the difference between the Fourier and non-Fourier consideration of heat conduction associated with the phase change in continuous casting examples.

The present paper is organized as follows: The hyperbolic formulation for the phase change problem is presented in Section 2. The finite element discretizations of the proposed formulation are presented in Section 3. Two- and three-dimensional numerical results are presented in Section 4, while Section 5 is devoted to the conclusion.

2. Mathematical model

In this section, we will briefly review the parabolic Stefan problem and the enthalpy formulation. Then, the derivation of the hyperbolic phase change model is presented.

2.1. Parabolic Stefan problem and the enthalpy formulation

The Stefan problem is the basic mathematical model for the solidification and melting of materials. It consists of the following equations:

$$
\begin{cases}
\rho_i c_i \dfrac{\partial T}{\partial t} - \nabla \cdot (\boldsymbol{K}_i \nabla T) & = f_i & \text{in } \Omega_i \ \ i = s, l \\[2mm]
T & = T_f & \text{on } \Gamma \\[2mm]
(\boldsymbol{K}_l \nabla T_l) \cdot \boldsymbol{n}_l - (\boldsymbol{K}_s \nabla T_s) \cdot \boldsymbol{n}_s = \rho_l L V_\Gamma & & \text{on } \Gamma
\end{cases}
\tag{1}
$$

where subscripts s and l refers to the solid and liquid phases, ρ_i is the density, c_i is the specific heat, $\boldsymbol{K}_i$ is the thermal conductivity tensor, f_i is a possible heat source, L is the latent heat of fusion, and V_Γ is the interface velocity.

The main difficulties in solving this system are the fact that the interface Γ and its velocity V_Γ are not known a priori and are also varying with time. The heat flux equilibrium condition often called the Stefan condition, must also be imposed. The classic way to avoid these difficulties in many numerical methods is the use of the enthalpy formulation for the simulation of phase change problems. It consists of the following set of equations:

$$
\frac{\partial H}{\partial t} - \nabla \cdot (K \nabla T) = f,
\tag{2}
$$

where the enthalpy H is a function of the temperature T and takes the form:

$$
H = F(T) =
\begin{cases}
\rho_s c_s T & \text{if} \quad T < T_f, \\[2mm]
\rho_s c_s T_f + \rho L + \rho_l c_l (T - T_f) & \text{if} \quad T > T_f.
\end{cases}
\tag{3}
$$

The conductivity $\boldsymbol{K}$ and the source term f are now given by:

$$
\boldsymbol{K} =
\begin{cases}
\boldsymbol{K}_s & \text{if } T < T_f, \\
\boldsymbol{K}_l & \text{if } T > T_f.
\end{cases}
\quad \text{and} \quad
f =
\begin{cases}
f_s & \text{if } T < T_f, \\
f_l & \text{if } T > T_f.
\end{cases}
$$

As illustrated in Fig. 2, the relation enthalpy-temperature has a discontinuity of height ρL and it can be shown that the problems (1) and (2) are equivalent, where the Stefan condition is automatically satisfied.

2.2. Derivation of hyperbolic phase change model

To consider the hyperbolicity, we will use a delayed flux for the material in the Stefan problem, as follows:

$$\begin{cases} \rho_i c_i \dfrac{\partial T}{\partial t} - \nabla \cdot \left(1 - \tau_i \dfrac{\partial}{\partial t}\right)(\boldsymbol{K}_i \nabla T) & = f_i & \text{in } \Omega_i \ \ i = s, l \\[2mm] T & = T_f & \text{on } \Gamma \\[2mm] \left(1 - \tau_l \dfrac{\partial}{\partial t}\right)(\boldsymbol{K}_l \nabla T_l) \cdot \boldsymbol{n}_l - \left(1 - \tau_s \dfrac{\partial}{\partial t}\right)(\boldsymbol{K}_s \nabla T_s) \cdot \boldsymbol{n}_s = \rho_l L V_\Gamma & \text{on } \Gamma \end{cases}$$

$$(4)$$

The equivalent enthalpy formulation to the above hyperbolic Stefan problem can be written as:

$$\frac{\partial H}{\partial t} - \nabla \cdot [(1 - \tau \partial_t)K\nabla T] = f. \tag{5}$$

Now, we will introduce a step function ϕ as follows

$$\phi = F(T) = \begin{cases} 0 & \text{in } \Omega_s, \\ 1 & \text{in } \Omega_l. \end{cases}$$

so that the enthalpy function can be written as

$$H = H_c + \rho_l L \phi,$$

where H_c is a continuous function:

$$H_c = \begin{cases} \rho_s c_s T & \text{in } \Omega_s, \\ \rho_s c_s T_f + \rho_l c_l (T - T_f) & \text{in } \Omega_l, \end{cases}$$

and therefore the enthalpy formulation can be re-written as

$$\frac{\partial H_c}{\partial t} + \rho L \frac{\partial \phi}{\partial t} - \nabla \cdot [(1 - \tau \partial_t)K\nabla T] = f,$$

where it is assumed that τ is the same for both phases. It is important to notice that a step function is considered for ϕ because of the step change in the enthalpy, which is characteristic of an isothermal or non-isothermal phase-change.

Considering the inverse approximation of the delayed flux (i.e., $(1 - \tau \partial_t)^{-1} \approx 1 + \tau \partial_t$), the energy balance becomes:

$$(1 + \tau \partial_t)\frac{\partial H_c}{\partial t} + \rho L (1 + \tau \partial_t)\frac{\partial \phi}{\partial t} - \nabla \cdot (K\nabla T) = (1 + \tau \partial_t)f.$$

This gives the second-order hyperbolic enthalpy formulation for the Stefan problem:

$$\frac{\partial H_c}{\partial t} + \tau \frac{\partial^2 H_c}{\partial t^2} + \rho L \frac{\partial \phi}{\partial t} + \tau \rho L \frac{\partial^2 \phi}{\partial t^2} - \nabla \cdot (K\nabla T) = f + \tau \frac{\partial f}{\partial t}.$$

Given that

$$\frac{\partial H_c}{\partial t} = \begin{cases} \rho_s c_s \dfrac{\partial T}{\partial t} & \text{in } \Omega_s, \\[2mm] \rho_l c_l \dfrac{\partial T}{\partial t} & \text{in } \Omega_l, \end{cases} \quad \text{and} \quad \frac{\partial^2 H_c}{\partial t^2} = \begin{cases} \rho_s c_s \dfrac{\partial^2 T}{\partial t^2} & \text{in } \Omega_s, \\[2mm] \rho_l c_l \dfrac{\partial^2 T}{\partial t^2} & \text{in } \Omega_l. \end{cases}$$

The final hyperbolic phase change model is given by

$$\begin{cases} \alpha(\phi)\dfrac{\partial T}{\partial t} + \tau \alpha(\phi)\dfrac{\partial^2 T}{\partial t^2} + \rho L \dfrac{\partial \phi}{\partial t} + \tau \rho L \dfrac{\partial^2 \phi}{\partial t^2} - \nabla \cdot (K(\phi)\nabla T) \\ = f(\phi) + \tau \dfrac{\partial f}{\partial t}(\phi), \\[2mm] \phi = F(T). \end{cases}$$

$$(6)$$

where:

$$\begin{cases} K(\phi) & = K_s + \phi(K_l - K_s), \\ \alpha(\phi) & = \rho_s c_s + \phi(\rho_l c_l - \rho_s c_s), \\ f(\phi) & = f_s + \phi(f_l - f_s), \\[2mm] \dfrac{\partial f}{\partial t}(\phi) & = \dfrac{\partial f_s}{\partial t} + \phi\left(\dfrac{\partial f_l}{\partial t} - \dfrac{\partial f_s}{\partial t}\right). \end{cases}$$

Notice that, if $\tau = 0$, we obtain the parabolic semi-phase-field model for simulation of phase problems as presented in Belhamadia et al. [29,30] and successfully compared with experimental results in Fortin and Belhamadia [31]. Also the above equations consider isothermal-phase-change. However, phase change may not not be instantaneous and occurs in a small interval $[T_f - \epsilon, T_f + \epsilon]$ where ϵ is a small parameter depending on the mushy region. Thus, the function $\phi = F(T)$ can be regularized in this interval so that the resulting function $\phi = F_\epsilon(T)$ considers both isothermal and non-isothermal phase-change.

The above model does not include the mechanism of heat convection. However, an extension of the present work is feasible following the ideas presented in Belhamadia et al. [32], El Haddad et al. [33].

2.3. Dimensionless form

To introduce the non-dimensional form of the model (6), we use the following change of variables. The dimensionless variables are represented with superscript $*$:

$$\boldsymbol{x}^* = \frac{\boldsymbol{x}}{\tilde{x}}, \qquad t^* = \frac{t}{\tilde{t}}, \quad \text{and} \quad T^* = \frac{T - T_f}{\Delta T},$$

where $\tilde{t}$, $\tilde{x}$, and ΔT are the reference time, length and temperature difference. ΔT can be chosen as any constant, relevant temperature difference, depending on the case considered. The same will be considered for $\tilde{x}$.

Using $\tilde{t} = \dfrac{\rho_l c_l \tilde{x}^2}{k_l}$, and the Stefan number $Ste = \dfrac{c_l \Delta T}{L}$, the dimensionless form of the model (6) is:

$$\begin{cases} \alpha^*(\phi)\dfrac{\partial T^*}{\partial t^*} + \tau^* \alpha^*(\phi)\dfrac{\partial^2 T^*}{\partial t^{*2}} + \dfrac{1}{Ste}\dfrac{\partial \phi}{\partial t^*} + \dfrac{\tau^*}{Ste}\dfrac{\partial^2 \phi}{\partial t^{*2}} \\ - \nabla \cdot (K^*(\phi)\nabla T^*) = f^*(\phi) + \tau^* \dfrac{\partial f^*}{\partial t^*}(\phi), \\[2mm] \phi = F(T^*). \end{cases} \tag{7}$$

where

$$\begin{cases} \boldsymbol{K}^*(\phi) & = \left(\dfrac{k_s}{k_l} + \phi\left(1 - \dfrac{k_s}{k_l}\right)\right)\boldsymbol{I}, \\[2mm] \alpha^*(\phi) & = \dfrac{\rho_s c_s}{\rho_l c_l} + \phi\left(1 - \dfrac{\rho_s c_s}{\rho_l c_l}\right) \\[2mm] f^*(\phi) & = \dfrac{f_s}{f_l} + \phi\left(1 - \dfrac{f_s}{f_l}\right), \\[2mm] \dfrac{\partial f^*}{\partial t^*}(\phi) & = \dfrac{\partial (f_s/f_l)}{\partial t^*}(1 - \phi), \\[2mm] \tau^* & = \dfrac{\tau k_l}{\rho_l c_l \tilde{x}^2}. \end{cases}$$

and the step function ϕ is given by

$$\phi = F(T^*) = \begin{cases} 0 & \text{if } T^* < 0, \\ 1 & \text{if } T^* > 0. \end{cases}$$

From here on, the dimensionless model (7) will be employed, and for simplicity, we will henceforward drop the symbol $(*)$ on all the variables.

3. Numerical method

A finite element method is used to numerically solve the hyperbolic phase-change model (7). The variational formulation of this system is straightforward and is obtained by multiplying the governing equation by a weighting function w and integrating over the computational domain Ω as follows:

$$\int_{\Omega} \left(\alpha(\phi) \frac{\partial T}{\partial t} w + \tau \alpha(\phi) \frac{\partial^2 T}{\partial t^2} w + \frac{1}{Ste} \frac{\partial \phi}{\partial t} w + \frac{\tau}{Ste} \frac{\partial^2 \phi}{\partial t^2} w \right.$$
$$\left. + (K(\phi)\nabla T) \cdot \nabla w)d\Omega = \int_{\Omega} \left(f(\phi)w + \tau \frac{\partial f}{\partial t}(\phi)w \right)d\Omega, \quad (8)$$

Homogeneous boundary conditions were considered for the temperature T to simplify the expression in (8). However, the general case can easily be obtained following the same lines.

The finite element discretization is based on quadratic polynomials for the temperature, which provides a second-order accuracy in space ($O(h^2)$). For the time derivatives, backward formulas are used for the first and second-order time derivatives. For instance, given the approximations T^{n-1}, T^n and T^{n+1} at times t^{n-1}, t^n and t^{n+1}, respectively, the first and second time derivatives at time t^{n+1} are approximated by:

$$\frac{\partial T}{\partial t}(t^{n+1}) \simeq \frac{T^{n+1} - T^n}{\Delta t} \text{ and } \frac{\partial^2 T}{\partial t^2}(t^{n+1}) \simeq \frac{T^{n+1} - 2T^n + T^{n-1}}{\Delta t^2}.$$

The variational formulation becomes:

$$\int_{\Omega} \left(\alpha(\phi^{n+1}) \left(\frac{T^{n+1} - T^n}{\Delta t} \right) + \tau \alpha(\phi^{n+1}) \left(\frac{T^{n+1} - 2T^n + T^{n-1}}{\Delta t^2} \right) \right)$$
$$w \, d\Omega + \int_{\Omega} K(\phi^{n+1})\nabla T^{n+1} \cdot \nabla w \, d\Omega = -\int_{\Omega} \left(\frac{1}{Ste} \left(\frac{\phi^{n+1} - \phi^n}{\Delta t} \right) \right.$$
$$\left. + \frac{\tau}{Ste} \left(\frac{\phi^{n+1} - 2\phi^n + \phi^{n-1}}{\Delta t^2} \right) \right) w \, d\Omega$$
$$+ \int_{\Omega} \left(f(\phi^{n+1}) + \tau \frac{\partial f}{\partial t}(\phi^{n+1}) \right) w \, d\Omega. \quad (9)$$

In the above system, we replaced ϕ^{n+1} with $F(T^{n+1})$, which makes the system nonlinear, and therefore Newton's method is employed at each time step. Iterative methods were used to solve the linear systems resulting from Newton's method. An incomplete *LU* decomposition (ILU) GMRES solver from the PETSc library is used [34].

For the case where $\tau = 0$, the numerical method (9) is the same as the one presented in Belhamadia et al. [29,30]. The approach was validated using an analytical solution in two and three-dimensional cases. It has also been validated using experimental data in Fortin and Belhamadia [31]. For the case where $\tau \neq 0$, the model has no analytical solution. However, we validated our approach using a manufactured solution and we obtained the expected theoretical order.

As we shall see, for a large value of τ the interfaces become sharper, and efficient numerical methods might be needed. Adaptive mesh methods as presented in Belhamadia et al. [35,36] can be employed. However, in this work we used fine meshes to get accurate results.

4. Numerical results

4.1. Experimental evidence of hyperbolic heat diffusion

The evidence of the hyperbolic behavior in heat diffusion has been experimentally shown in the literature. In particular, experimental data on heat propagation in processed meat for different
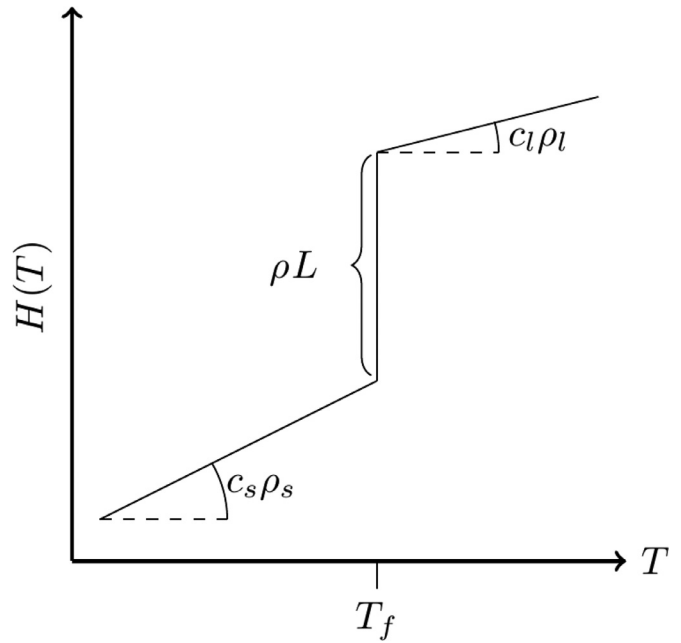
Fig. 1. Enthalpy-temperature relation in a phase change problem.

Table 1
Parameters used for the reproduction of the results from Mitra et al. [37]

Case I			Case II		
Parameter	Value	Unit	Parameter	Value	Unit
α	1		α	1	
$\tilde{t}$	284	s	$\tilde{t}$	161.161	s
$T_0(x,y)$	0		$T_0(x,y)$	$= \begin{cases} 0, & \text{for } 0 < x < 1 \\ 2, & \text{for } 1 < x < 4 \end{cases}$	
x_o	1		x_o	0.2	
L_x	3		L_x	4	
L_y	1		L_y	1	
τ	0.0556		τ	0.0962	

conditions can be found in Mitra et al. [37]. Although there is no phase change in this example, the data shows the finite speed of propagation of the heat wave through the solid body with a delay in the response. First, we will numerically illustrate the evidence of the hyperbolic behavior by comparing our numerical results using both the parabolic and hyperbolic heat diffusion with the experimental data available in Mitra et al. [37].

Our numerical results will be compared to two experimental cases examined in Mitra et al. [37]. The first case considers two identical samples at different initial temperatures brought into contact with each other. One sample is initially refrigerated (temperature of $T_C = 1$ (8.2 °C)) and the other is at room temperature ($T_r = 0$ (23.1 °C)). A thermocouple is embedded in the room temperature sample at $x = 1$ (6.3 mm) from the interface of contact (see the left side of Fig. 2). In the second case, three samples are brought into contact, two initially refrigerated ($T_C = 1$ (8.5 °C)) and one at room temperature ($T_r = 0$ (17.4 °C)), such that the body at room temperature is in between the refrigerated ones. The room temperature sample has a length of 2 (9.5 mm), and a thermocouple is placed inside it at $x = 0.2$ (0.95 mm) from the middle of it (see the right side of Fig. 2). For both cases, the reference temperature difference used in the dimensionalization is $\Delta T = T_C - T_r$. So, $\Delta T = -14.9$ °C for case 1 and $\Delta T = -8.9$ °C for case 2.

The physical parameters considered for these two cases are summarized in Table 1. For the first case, the comparison between the experimental and simulation results is shown in Fig. 3. As can be seen in this figure, the experimental results show that the heat
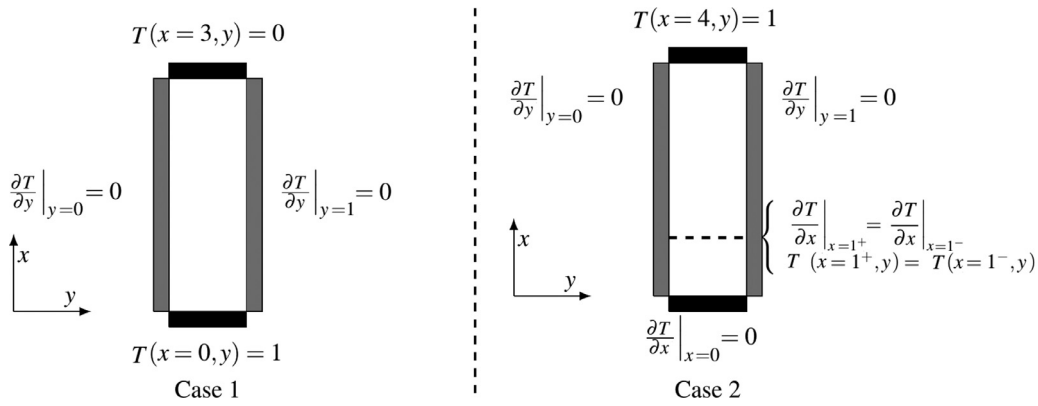
Fig. 2. "Mitra et al." [37]: Cases 1 and 2.
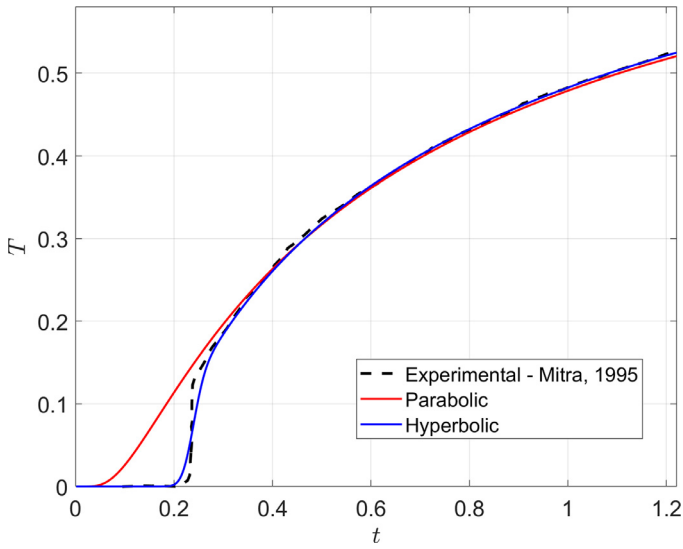
Fig. 3. Comparison between the experimental and simulation results: Thermal profile at $x = 1$ for case 1.
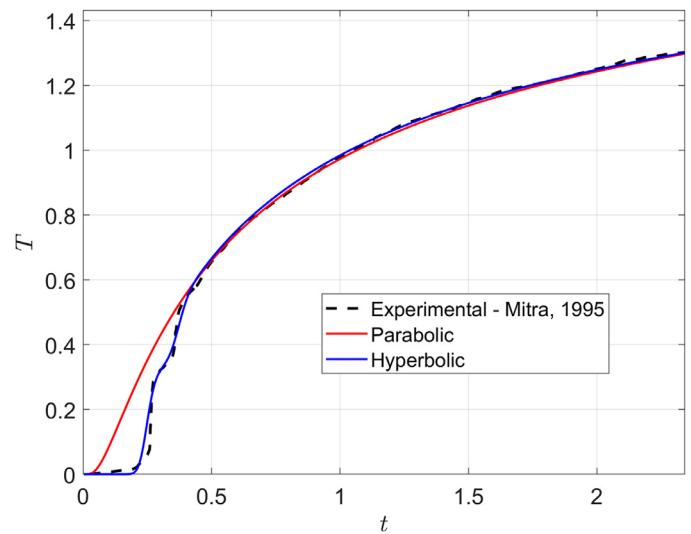
Fig. 4. Comparison between the experimental and simulation results: Thermal profile at $x = 0.2$ for case 2.

waves take a finite time to reach a particular point inside the sample, which is not predicted by the instantaneous heat propagation using the Fourier flux. Thus, the numerical temperature profile obtained with the parabolic model does not show the behavior expected. However, the hyperbolic model provides good results in comparison with the experimental data.

For the second case, the comparison between the experimental and simulation results is shown in Fig. 4. The experimental data clearly shows two temperature jumps associated with the two wavefronts originated from the interfaces between the room temperature sample and the two cold samples. As can be observed in this figure, the presence of the two jumps cannot be obtained by Fourier flux and the associated parabolic PDE. However, this behavior is well obtained via heat waves represented by the hyperbolic model.

It is worth mentioning that the value of τ in the hyperbolic model is experimentally estimated from the non-dimensionless data by noting the instant at which the imposed temperature boundary condition causes the measured data to be significantly different from the initial temperature.

The results of the experiments described above offer compelling evidence of the finite wave speed nature of heat conduction. The fact that a finite time occurs before the thermocouples embedded within the media register any temperature deviations, and that the temperature changes abruptly indicate a wave behavior of the con-
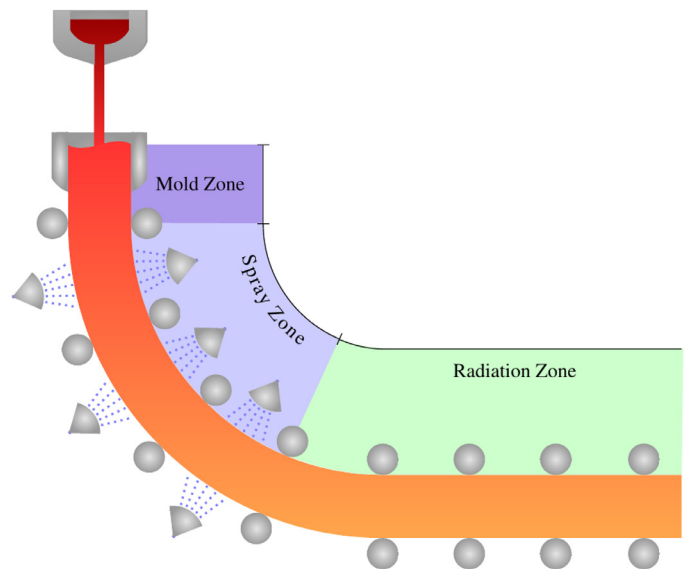
Fig. 5. Representation of the continuous steel casting process. The black lines represent the sampled regions shown in the simulations results.

$$\left.\frac{\partial T}{\partial y}\right|_{y=L_y/2} = q_m$$

$$\left.\frac{\partial T}{\partial x}\right|_{x=0} = 0 \qquad \left.\frac{\partial T}{\partial x}\right|_{x=L_x/2} = q_m$$

$$\left.\frac{\partial T}{\partial y}\right|_{y=0} = 0$$
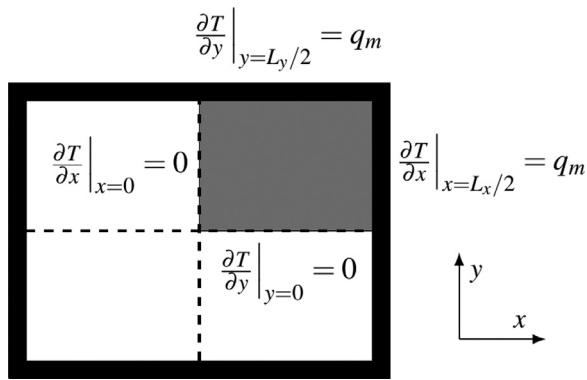
Fig. 6. Simplified 2D case in the continuous casting mold zone.

Table 2
Dimensionless parameters for the simplified 2D case.

Parameter	Value
T_f	0
T_a	-0.9737705
T_0	0.02623
$k_s(T)$	$35.512 + 16.775T$
h_m	$\frac{230.79}{35.512+16.775T}$
$\frac{k_s}{k_l}$	0.5
$\frac{\rho_s c_s}{\rho_l c_l}$	1
Ste	3.82

duction mechanism. These phenomena are clearly evident from the experimental data shown in Figs. 3 and 4 and clearly obtained with the hyperbolic approach rather than the parabolic one.

For phase change problems, there is a jump in the enthalpy at the interface position, as shown in Fig. 1. This delays the propagation of the heat between the liquid and solid phases, which makes the hyperbolic approach more suitable for these types of problems, as will be presented in the following examples.

4.2. Solidification of steel

In continuous casting, metal is heated until it liquefies, then the molten metal is cast through a mold and is solidified as it keeps traveling downward. The molten metal is continuously supplied to the mold at the same rate to match the solidifying casting. The beam is continuously drawn into a partially solidified billet, bloom, or slab, such that the process allows the casting of slabs with uninterrupted lengths and long strands of metal [38].

Due to the high complexity and danger of the operation, a carefully controlled process is necessary to reduce errors and lead to better quality steel casts, which increases productivity and yields. Appropriate numerical modeling of continuous casting is thus fundamental for better understanding the process and enhancing steel productivity. The thermal transport phenomenon plays a key role in this process and needs to be accurately modeled as a phase change problem since the material changes from a state of liquid to a solid.

Generally, three different cooling zones are considered in this process: The mold (wall) cooling zone, or the primary zone, which gives the initial shape of the steel beam. The spray cooling zone controls the cooling of the solidifying strand as it progresses through the continuous casting machine. Then the radiation zone counts for heat lost through thermal radiation.

In our numerical simulation, we will consider a two-dimensional simplification case to simulate the solidification process in the primary zone. Then, a three-dimensional case also presenting the spray and radiation zones will be considered to show the difference between the hyperbolic and parabolic approaches in phase change problems.

4.2.1. Simplified 2D model - mold zone

The primary zone has the highest temperature difference in the continuous casting process. The solidification process in this zone is a crucial step where all the external walls of the steel should be solidified by the end of the mold zone for the continuity of the rest of the casting process. Thus, accurate simulation of this primary zone is essential, not only due to the initial temperature difference. As we shall see, the difference between hyperbolic and parabolic equations will be more evident.

To simulate the solidification process in the primary zone of the continuous casting, we will first consider the mold temperature to be at steady-state, assuming the mold diffusivity is much higher than the steel (see Kumar et al. [39]) and therefore, the process can be simplified to only a two-dimensional heat transfer problem. Also, as shown in Fig. 6, only a one-quarter model can be considered as the heat transfer problem is symmetric. The heat transfer coefficient between the steel and the environment through the mold can be defined as:

$$q_m = h_m(T_a - T) \tag{10}$$

All other dimensionless parameters needed for the simulation are presented in Table 2 using $\tilde{x} = L_x = L_y$, $\tilde{t} = \frac{\rho c_P \tilde{x}^2}{k_l(T_0)} \approx 18\,\text{s}$, and $\Delta T = T_0 - T_a = 1525\,\text{K}$.

The material is initially in a melted state, just above the melting point, and the boundaries are at a temperature lower than the melting point. Therefore, the mold starts to solidify with time, and the surface begins to cool down immediately. The numerical results are presented in Fig. 7. The three cases correspond to $\tau = 0$, $\tau = 0.005$, and $\tau = 0.01$. The case where $\tau = 0$ corresponds to the commonly used parabolic approach. As can be observed in this figure, the heat transfer throughout the surface is more pronounced in the case $\tau = 0$, and the solidification front moves faster when compared to the numerical results obtained for $\tau = 0.005$ and $\tau = 0.01$. Furthermore, the temperature profile is sharper for the larger value of τ. This is clearly seen in the temperature profiles, where the edges of the solutions for $\tau = 0.01$ are distinguishable. This is expected from the wave-like behavior of the hyperbolic equation and the non-Fourier damped heat flux.

The difference in the heat propagation is not only seen in the solidification of the steel but also in the propagation in the solidified phase. For $\tau = 0.01$, the initial temperature difference takes longer to dissipate, which can be seen for $t = 0.005$ and $t = 0.05$ in the last row of Fig. 7, where the temperature distribution is still sharpened in the corner. For $\tau = 0$, the temperature difference in the corner is rapidly dissipated, and by $t = 0.1$, the corner effects are not noticeable.

Similar to the problem analyzed in the previous section, the differences between results in the Fourier model and the non-Fourier heat conduction model should decrease at increasing times and tend to disappear as t increases. This is perceptible when comparing figures in the last column in Fig. 7, where the difference between the temperature profiles is less discernible. However, the difference in the temperature distribution at the corners still is evident.

Figure 8 shows the difference in the interface dynamics for the three values of τ. The interface position is clearly affected by the value of the τ mainly because the heat diffusion is initially faster as τ goes to zero. Thus, the body cools down faster for, for instance, $\tau = 0.005$, and the dynamic of the interface follows a similar trend when compared to the interface position for $\tau = 0.01$.
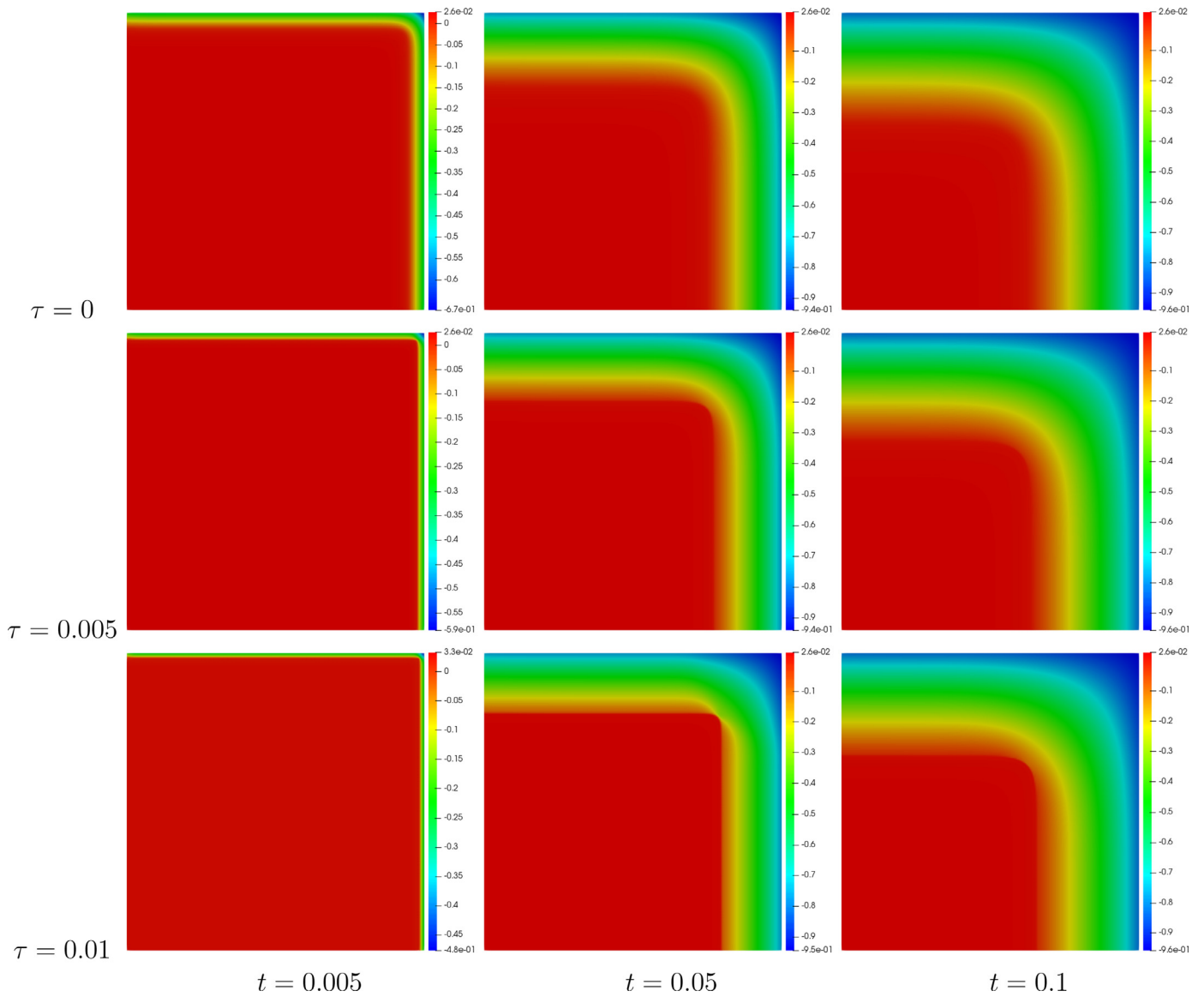
Fig. 7. Temperature profile of the 2D steel solidification in 2D in different time instances for $\tau = 0$, $\tau = 0.005$, and $\tau = 0.01$. The temperature profile is sharper for the larger value of τ.
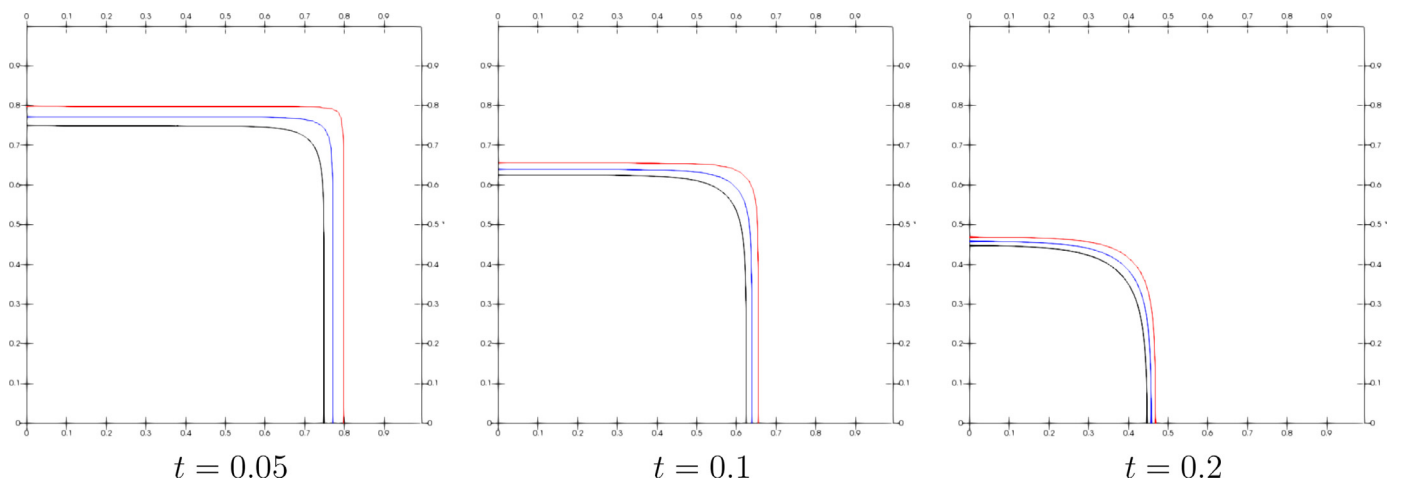
Fig. 8. Interface position at different time instances for $\tau = 0$ (black curve), $\tau = 0.05$ (blue curve), and $\tau = 0.1$ (red curve). (For interpretation of the references to color in this figure legend, the reader is referred to the web version of this article.)
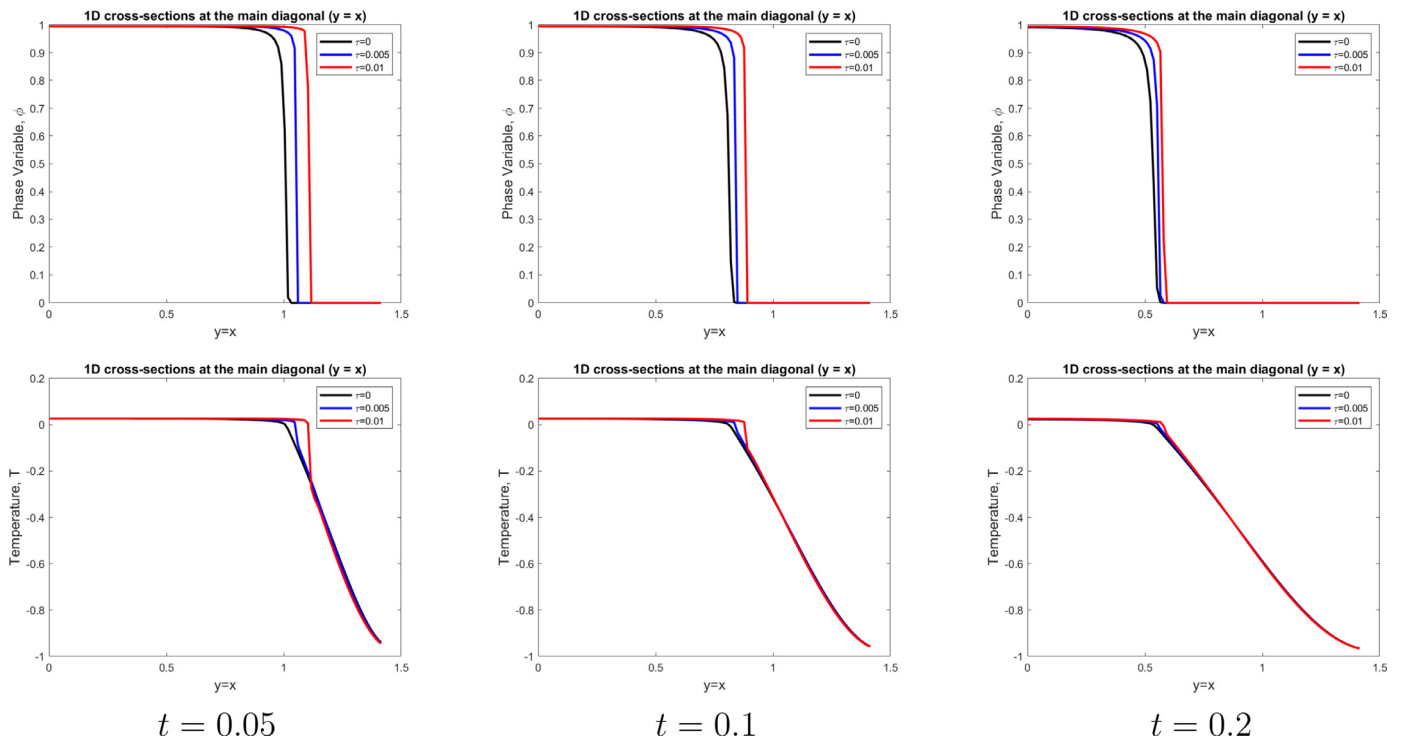
Fig. 9. 1D cross section at the diagonal $y = x$ for both variables T and ϕ.
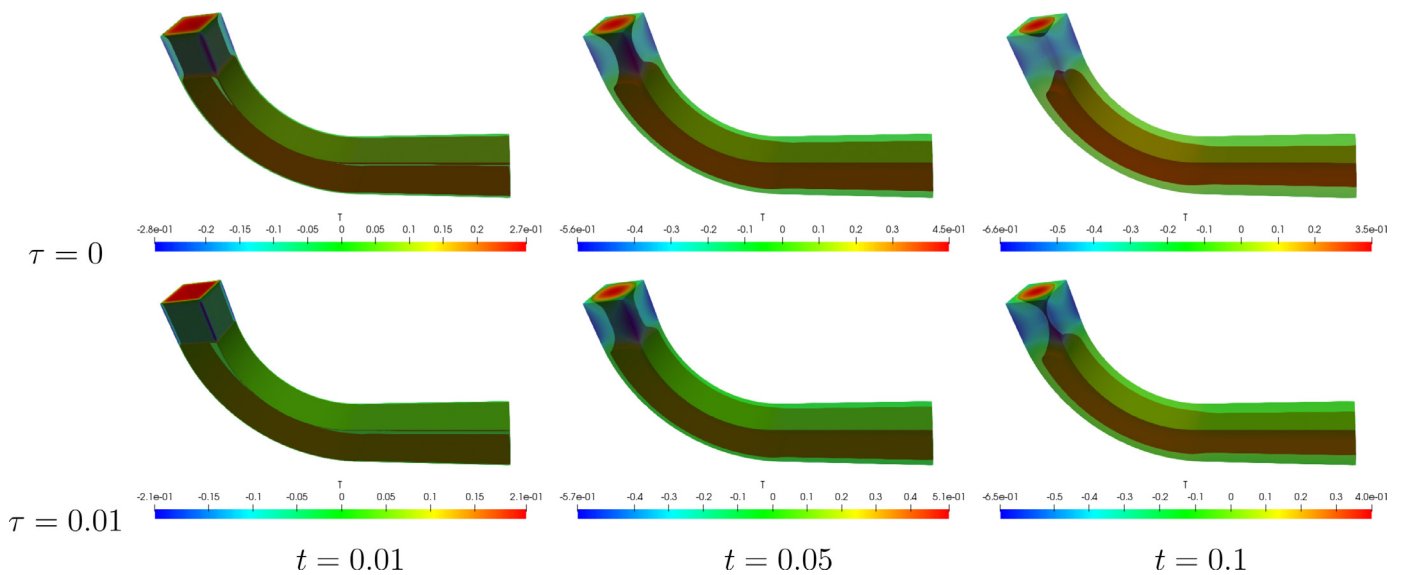
Fig. 10. Tthree-dimensional simulation results in different time instances for $\tau = 0$, and $\tau = 0.01$.

This is also observed in Fig. 9 where the 1D cross section at the main diagonal $y = x$ for both variables T and ϕ is presented.

Once again, as expected, the differences between the two types of heat conduction decrease at increasing times and tend to disappear as t is getting larger and this effect is more easily noticeable when analyzing the interface dynamics.

4.2.2. Complete 3D model

In this section, the complete 3D model (as shown in Fig. 5) is considered. The parameters used were taken from Kumar et al. [39] and are summarized in Table 3. The dimensionless parameters considered are $\tilde{x} = 0.14\,\text{m}$, $\tilde{t} = \frac{\rho c \tilde{x}^2}{k_l} = 2060\,\text{s}$, and $\Delta T = T_0 - T_a = 1533\,\text{K}$.

Table 3
Parameters used for the 3D case.

Parameter	Value
T_f	0
T_a	−0.9501
T_0	0.05
$\frac{k_s}{k_l}$	1.4984
$\frac{\rho_s c_s}{\rho_l c_l}$	0.9375
γ	1.1445
Ste	3.7735
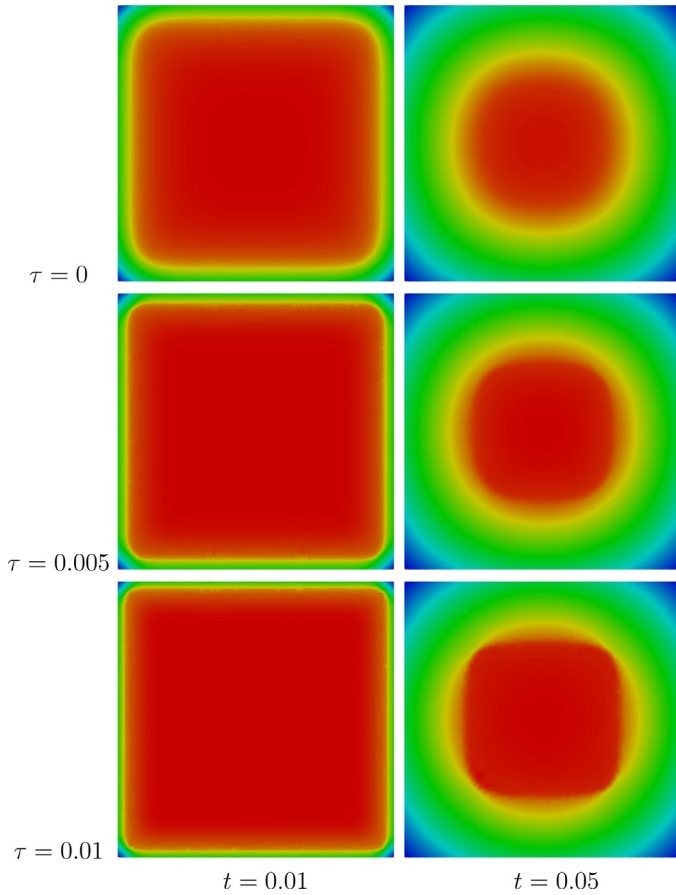
Fig. 11. Temperature profile at a cross section of the primary zone region for $\tau = 0$, $\tau = 0.005$, and $\tau = 0.01$.
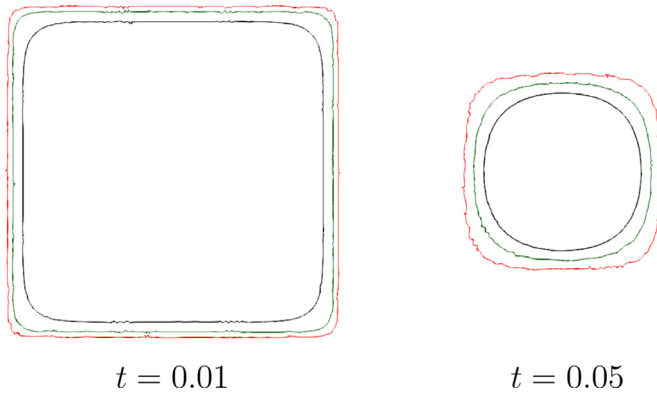
Fig. 12. Interface position at a cross-section of the primary zone region for $\tau = 0$ (black curve), $\tau = 0.005$ (green curve) and $\tau = 0.01$ (red curve). (For interpretation of the references to color in this figure legend, the reader is referred to the web version of this article.)

At the boundary, the beam is considered as solid, $k = k_{sol}$. In the mold zone, the following boundary condition is used:

$$\partial T|_\Gamma = -3.1896[T|_\Gamma - T_a] \tag{11}$$

A similar type of boundary condition is used in the spray zone:

$$\partial T|_\Gamma = -0.4870[T|_\Gamma - T_a] \tag{12}$$

and for the radiation zone:

$$\partial T|_\Gamma = -0.4974\Big\{ (T|_\Gamma)^4 - (T_a)^4 + 4\gamma[(T|_\Gamma)^3 - (T_a)^3] \\ +6\gamma^2[(T|_\Gamma)^2 - (T_a)^2] + 4\gamma^3[(T|_\Gamma) - (T_a)] \Big\} \tag{13}$$

Homogeneous boundary conditions are used on the left and right sides for both spray and radiation zones. To make a better assessment of the difference between the models, both the temperature distribution and the interface dynamics are considered. Figure 10 shows three-dimensional plots of the temperature distribution and the position of the interface corresponding to the surface $\phi = 0.5$ using two values of τ: $\tau = 0$ and $\tau = 0.01$. The case where $\tau = 0$ corresponds to the commonly used parabolic approach. As can be observed in this figure, the heat transfer throughout the surface is more pronounced in the case $\tau = 0$, and the solidification front moves faster when compared to the numerical results obtained with $\tau = 0.01$. This is clearly shown in the last column of Fig. 10.

Furthermore, the temperature profile is sharper for the higher value of τ. This is shown in Figs. 11 and 12 where the temperature profile and the interface curves at a cross-section of the primary zone region are presented for value $\tau = 0$, $\tau = 0.005$, and $\tau = 0.01$, as it can be observed, the edges of the hyperbolic equation solutions for $\tau = 0.01$ are distinguishable. This is expected from the wave-like behavior of the hyperbolic equation and the non-Fourier damped heat flux. It can also be observed that for $\tau = 0.01$, the initial temperature difference takes longer to dissipate, as shown in the interface position at time $t = 0.01$ in Fig. 12. For $\tau = 0$, the temperature difference in the corner is rapidly dissipated, and by $t = 0.05$, the corner effects are not noticeable.

5. Conclusions

Although the infinite speed paradox may be ignored in some applications, there are many other heat transfer applications where a finite speed of propagation is observed. In this paper, we proposed a hyperbolic heat diffusion mathematical model for simulating the finite speed of heat propagation in phase change problems with application to steel continuous casting. We first illustrated the difference between the infinite and finite velocity of propagation in biological tissues, where numerical and experimental results were compared. Then, we presented two and three-dimensional numerical results in the case of a continuous steel casting process. The difference between parabolic and hyperbolic approaches was clearly illustrated. First, we showed a clear difference in the initial thermal dynamic and that the temperature profile is sharper for the larger value of τ in the hyperbolic model. We also illustrated the difference in the solid-liquid interface when simulating a continuous steel casting process. We concluded that the hyperbolic leads to a distinctive temperature behavior when the solidification happens faster in the mold region. Although we considered continuous casting as an example, our model and methodology are general and can be applied to other phase change problems. Numerically, for a large value of τ, the interfaces become sharper, and efficient numerical methods might be needed. Adaptive mesh methods can be used, and this will be a subject of a future work. In addition, it will be interesting to couple the proposed model in this paper with the mechanism of heat convection.

Declaration of Competing Interest

The authors declare that they have no known competing financial interests or personal relationships that could have appeared to influence the work reported in this paper.

CRediT authorship contribution statement

Youssef Belhamadia: Conceptualization, Formal analysis, Funding acquisition, Methodology, Resources, Software, Validation, Writing – review & editing. **Guilherme Ozorio Cassol:** Conceptualization, Formal analysis, Methodology, Writing – review & edit-

ing. **Stevan Dubljevic:** Conceptualization, Formal analysis, Funding acquisition, Methodology, Supervision, Writing – review & editing.

Data availability

No data was used for the research described in the article.

Acknowledgments

References

[1] H. Gomez, I. Colominas, F. Navarrina, J. Paris, M. Casteleiro, A hyperbolic theory for advection-diffusion problems: mathematical foundations and numerical modeling, Arch. Comput. Methods Eng. 17 (2010) 191–211.

[2] C.I. Christov, P.M. Jordan, Heat conduction paradox involving second-sound propagation in moving media, Phys. Rev. Lett. 94 15 (2005) 154–301.

[3] D. Tzou, Y, D, Macro- To Micro-Scale Heat Transfer: The Lagging Behavior, Chemical and Mechanical Engineering Series, Taylor & Francis, 1996. https://www.books.google.ca/books?id=J1bzz7sDln4C

[4] J. Li, Y. Gu, Z. Guo, Analysis of the phenomena of non-Fourier heat conduction in switch-q laser processing for reducing the core loss of grain-oriented silicon steel, J. Mater. Process. Technol. 74 (1) (1998) 292–297.

[5] A. Banerjee, A.A. Ogale, C. Das, K. Mitra, C. Subramanian, Temperature distribution in different materials due to short pulse laser irradiation, Heat Transf. Eng. 26 (8) (2005) 41–49.

[6] C. Cattaneo, On a form of heat equation which eliminates the paradox of instantaneous propagation, C. R. Acad. Sci. Paris 247 (1958) 431–433.

[7] T.F. Nonnenmacher, Derivation of exact non-linear constitutive equations: a simple model for a non-linear diffusion theory, J. Non-Equilibrium Thermodyn. 9 (3) (1984) 171–176.

[8] S. Godoy, L.S. Garcia-Colin, From the quantum random walk to classical mesoscopic diffusion in crystalline solids, Phys. Rev. E 53 (1996) 5779–5785.

[9] A.C. King, D.J. Needham, N.H. Scott, The effects of weak hyperbolicity on the diffusion of heat, Proc.: Math., Phys. Eng. Sci. 454 (1974) (1998) 1659–1679.

[10] I. Novikov, Solution of the linear one-dimensional inverse heat-conduction problem on the basis of a hyperbolic equation, J. Eng. Phys. 40 (1981) 668–672.

[11] M. Fabrizio, B. Lazzari, Stability and second law of thermodynamics in dual-phase-lag heat conduction, Int. J. Heat Mass Transf. 74 (2014) 484–489.

[12] J. Porra, J. Masoliver, G. Weiss, When the telegrapher's equation furnishes a better approximation to the transport equation than the diffusion approximation, Phys. Rev. E 55 (1997) 7771–7774.

[13] S. Rukolaine, Unphysical effects of the dual-phase-lag model of heat conduction, Int. J. Heat Mass Transf. 78 (2014) 58–63.

[14] T. Bright, Z. Zhang, Common misperceptions of the hyperbolic heat equation, J. Thermophys. Heat Transf. 23 (3) (2009) 601–607.

[15] D. Maillet, A review of the models using the Cattaneo and Vernotte hyperbolic heat equation and their experimental validation, Int. J. Therm. Sci. 139 (2019) 424–432.

[16] S. Both, B. Czél, T. Fülöp, G. Gróf, Á Gyenis, R. Kovács, P. Ván, J. Verhás, Deviation from the Fourier law in room-temperature heat pulse experiments, J. Non-Equilibrium Thermodyn. 41 (1) (2016) 41–48.

[17] V. Surov, Hyperbolic model of a single-speed, heat-conductive mixture with interfractional heat transfer, High Temp. 56 (2018) 890-899.

[18] O. Nosko, Hyperbolic heat conduction at a microscopic sliding contact with account of adhesion-deformational heat generation and wear, Int. J. Therm. Sci. 137 (2019) 101–109.

[19] G. Abbasi, A. Malek, Pointwise optimal control for cancer treatment by hyperthermia with thermal wave bioheat transfer, Automatica 111 (2020) 108579.

[20] S. Rossi, B.E. Griffith, Incorporating inductances in tissue-scale models of cardiac electrophysiology, Chaos 27 (9) (2017) 093926.

[21] O. Nosko, Perfect thermal contact of hyperbolic conduction semispaces with an interfacial heat source, Int. J. Heat Mass Transf. 164 (2021) 120541, doi:10.1016/j.ijheatmasstransfer.2020.120541. https://www.sciencedirect.com/science/article/pii/S0017931020334773

[22] A. Fehér, R. Kovács, Analytical evaluation of non-Fourier heat pulse experiments on room temperature, IFAC Workshop on Thermodynamic Foundations of Mathematical Systems Theory, 2022.

[23] L. Rubenstein, The Stefan Problem, Translations of Mathematical Monographs, American Mathematical Society, 1971.

[24] L. de Socio, G. Gualtieri, A hyperbolic Stefan problem, Q. Appl. Math. 41 (1983), doi:10.1090/qam/719509.

[25] R. Showalter, N. Walkington, A hyperbolic Stefan problem, Q. Appl. Math. XLV (4) (1987) 769–781.

[26] D.E. Glass, M.N. Ozisik, W.S. Kim, Hyperbolic Stefan problem with applied surface heat flux and temperature-dependent thermal conductivity, Numer. Heat Transf., Part A 18 (4) (1991) 503–516.

[27] Jitendra, K.N. Rai, J. Singh, A numerical study on non-Fourier heat conduction model of phase change problem with variable internal heat generation, J. Eng. Math. 129 (7) (2021).

[28] A. Kumar, S. Kumar, V. Katiyar, S. Telles, Phase change heat transfer during cryosurgery of lung cancer using hyperbolic heat conduction model, Comput. Biol. Med. 84 (2017) 20–29.

[29] Y. Belhamadia, A. Fortin, É. Chamberland, Anisotropic mesh adaptation for the solution of the Stefan problem, J. Comput. Phys. 194 (1) (2004) 233–255.

[30] Y. Belhamadia, A. Fortin, É. Chamberland, Three-dimensional anisotropic mesh adaptation for phase change problems, J. Comput. Phys. 201 (2) (2004) 753–770.

[31] A. Fortin, Y. Belhamadia, Numerical prediction of freezing fronts in cryosurgery: Comparison with experimental results, Comput. Methods Biomech. Biomed. Eng. 8 (4) (2005) 241–249.

[32] Y. Belhamadia, A.S. Kane, A. Fortin, An enhanced mathematical model for phase change problems with natural convection, Int. J. Numer. Anal. Model. Ser. B 3 (2) (2012) 192–206.

[33] M. El Haddad, Y. Belhamadia, J. Deteix, D. Yakoubi, A projection scheme for phase change problems with convection, Comput. Math. Appl. 108 (2022) 109–122, doi:10.1016/j.camwa.2022.01.001. https://www.sciencedirect.com/science/article/pii/S0898122122000013

[34] S. Balay, S. Abhyankar, M.F. Adams, S. Benson, J. Brown, P. Brune, K. Buschelman, E.M. Constantinescu, L. Dalcin, A. Dener, V. Eijkhout, J. Faibussowitsch, W.D. Gropp, V. Hapla, T. Isaac, P. Jolivet, D. Karpeev, D. Kaushik, M.G. Knepley, F. Kong, S. Kruger, D.A. May, L.C. McInnes, R.T. Mills, L. Mitchell, T. Munson, J.E. Roman, K. Rupp, P. Sanan, J. Sarich, B.F. Smith, S. Zampini, H. Zhang, H. Zhang, J. Zhang, PETSc Web page, 2022, (https://petsc.org/). https://petsc.org/.

[35] Y. Belhamadia, A. Fortin, T. Briffard, A two-dimensional adaptive remeshing method for solving melting and solidification problems with convection, Numer. Heat Transf., Part A 76 (4) (2019) 179–197.

[36] Y. Belhamadia, T. Briffard, A. Fortin, Efficiency of parallel anisotropic mesh adaptation for the solution of the bidomain model in cardiac tissue, J. Comput. Sci. 61 (2022) 101656, doi:10.1016/j.jocs.2022.101656. https://www.sciencedirect.com/science/article/pii/S1877750322000709

[37] K. Mitra, S. Kumar, A. Vedevarz, M.K. Moallemi, Experimental evidence of hyperbolic heat conduction in processed meat, J. Heat Transf. 117 (3) (1995) 568–573.

[38] S. Louhenkilpi, Chapter 1.8 - continuous casting of steel, in: S. Seetharaman (Ed.), Treatise on Process Metallurgy, Elsevier, Boston, 2014, pp. 373–434.

[39] M. Kumar, S. Roy, S.S. Panda, Numerical simulation of continuous casting of steel alloy for different cooling ambiences and casting speeds using immersed boundary method, Proc. Inst. Mech. Eng., Part B 231 (8) (2017) 1363–1378.